ID: EGU2017-44

Spectral descriptions of submesoscale surface circulation in a coastal region off the East Coast of Korea

Jang Gon Yoo[1], Sung Yong Kim[1,†], and Hyeon Seong Kim[2]

[1]Department of Mechanical Engineering Korea Advanced Institute of Science and Technology, [2]KOSEC-Tech, Corp, Seoul 08381, Republic of Korea

syongkim@kaist.ac.kr[†]

Mechanical Engineering KAIST

Ministry of Oceans and Fisheries

Ministry of Public Safety and Security

Abstract

The spectral characteristics of hourly and 1-km resolution coastal surface currents obtained from an array of high-frequency radars of a coastal region off the East Coast of Korea are described in the frequency and wavenumber domains. The primary variance of the observed surface currents for a period of one year appears in the low-frequency (longer than 2 days), diurnal, and near-inertial frequency bands. The low-frequency surface currents exhibit more consistent variability with the regional geostrophic currents in summer than those in winter because of the relatively weaker wind conditions and a shallower mixed layer during summer. The diurnal surface circulation contains components that are coherent with diurnal land-sea breezes because of the development of the diurnal marine boundary layer. Clockwise near-inertial surface currents show onshore phase propagations along with their decreasing amplitudes, represented as a coastal inhibition associated with coastal boundary effects on the near-inertial currents in coastal areas. The kinetic energy spectra of the surface currents in the wavenumber domain have decay slopes between k^{-2} and k^{-3}, and their seasonal decay slopes are slightly steeper in winter than in summer. These findings can be interpreted that the submesoscale processes in this region can be related to both surface frontogenesis caused by regional mesoscale eddies with weak seasonality and baroclinic instability associated with the seasonal mixed layer and vertical fluctuations modulated by its harmonic frequencies.

Observations

Hourly averaged surface currents on a grid with a 1 km spatial resolution off the coast of Imwon, Republic of Korea for a period of one year (2013) have been obtained by two phased-array HFRs [WavE RAdar (WERA) system] of Imwon North (IMWN; R1) and Imwon South (IMWS; R2) (Figure 2b). Although the WERA-derived radial velocities are typically reported on a Cartesian coordinate grid for the convenience of vector current mapping, we internally modify scripts and obtain the radial velocities reported on the polar coordinate grids of individual HFRs, which allows us to investigate the characteristics of the radial velocity data prior to mapping and apply optimal interpolation (OI) to directly estimate the kinematic and dynamic quantities (e.g., stream function, velocity potential, divergence, vorticity, and strain rates) of surface currents with any intermediate steps. In this paper, OI uses an exponential correlation functions with an isotropic decorrelation length scales of 1.5 km to minimize spatial smoothing [[1]].

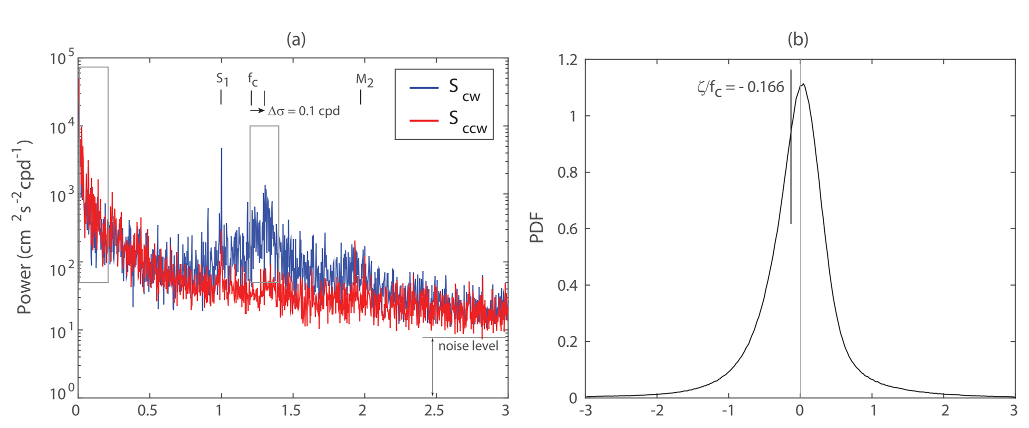

Figure 1: (a) Frequency-domain rotary spectra of the hourly surface vector currents are presented in the clockwise (S_{cw}) and counter-clockwise (S_{ccw}) rotations, averaged over 553 grid points (a gray curve in Figure 2b). A black line indicates the local inertial frequency ($f_c = -1.2078$ cpd at 37.15°N), and two gray boxes denote the non-zero low-frequency band ($0 < |\sigma| \leq 0.2$ cpd) and clockwise near-inertial frequency band ($-1.4 \leq \sigma \leq -1.2$ cpd). A super-inertially shifted peak appears in the clockwise rotation, $\delta f = -0.1$ cpd. The noise level is defined as the floor level at the Nyquist frequency (12 cpd). (b) A probability density function of the normalized vorticity (ζ/f_c). The normalized vorticity of -0.166 ($\zeta/f_c = -0.166$) is marked.

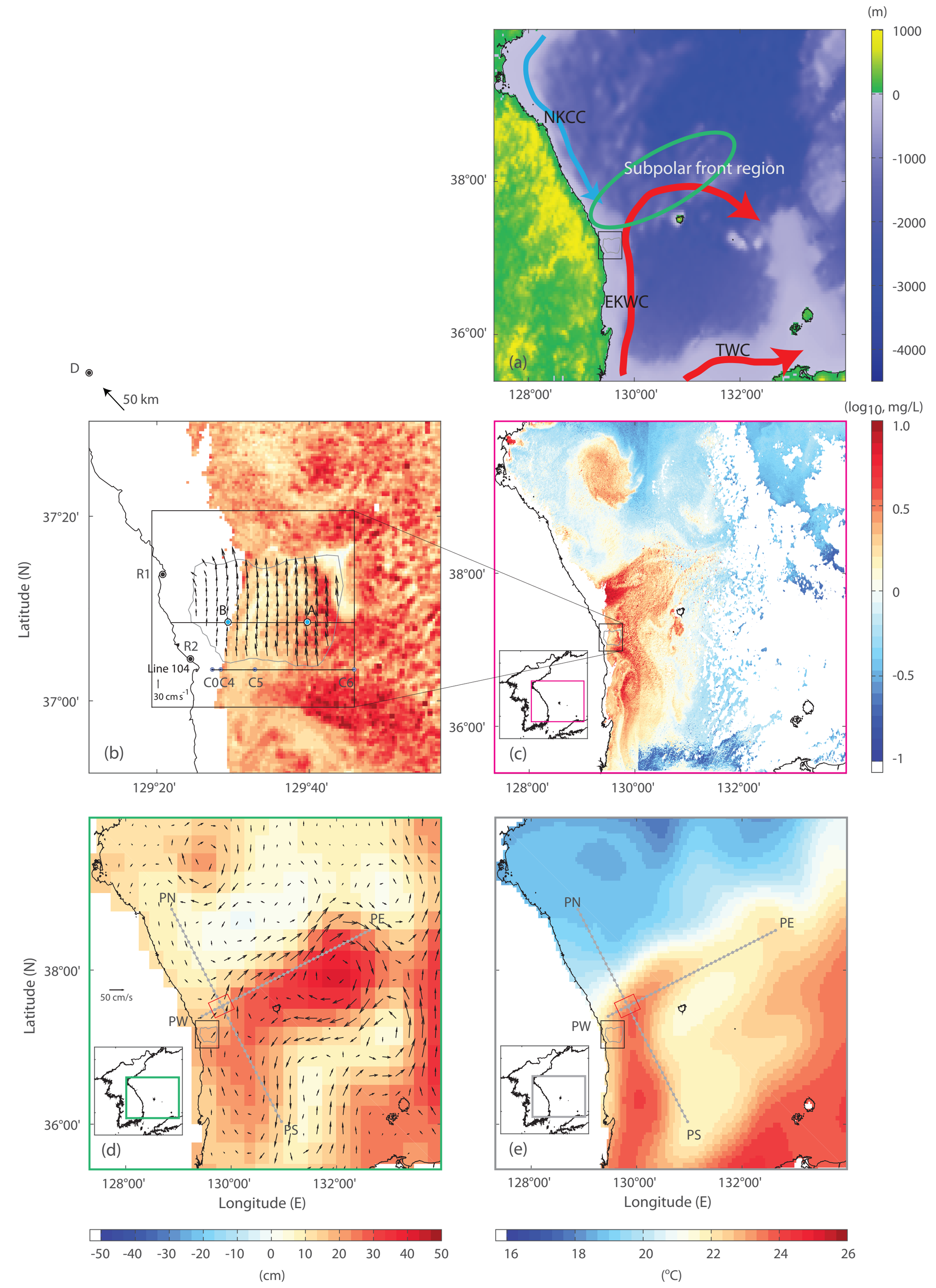

Figure 2: (a) Schematic regional circulation off the East Coast of Korea shows the North Korea Cold Current (NKCC), East Korea Warm Current (EKWC), Tsushima Warm Current (TWC), and the subpolar front region, overlaid on the bottom bathymetry (m). (b) to (e): An example of (b) the coastal high-frequency radar (HFR)-derived surface current map on a 2-km resolution grid, (c) the chlorophyll concentration map (GOCI L2A products) on a 0.5-km resolution grid ($\log_{10}$ scale, $\mathrm{mg\,L^{-1}}$), (d) the AVISO sea surface height anomaly (SSHA, cm) and geostrophic current maps on the quarter degree resolution grid, and (e) the sea surface temperature [SST (OSTIA UKMO); °C] map on a 0.05-degree resolution grid off Imwon, Republic of Korea. The HFR-derived surface currents and the chlorophyll concentration are sampled at 16:40 (GMT) on October 12, 2013, and the AVISO products and the SST are optimally interpolated at the time centered by October 12, 2013 (GMT).

Variance in the frequency domain

The temporal mean ($\sigma = 0$ cpd) and standard deviation of the surface currents over a period of one year (2013) show spatially uniform northward flows along with significant offshore variability (Figure 3a), which is a part of the persistent northward EKWC [e.g., [2]].

The low-frequency surface currents are relatively enhanced offshore and reduced nearshore (Figure 3b), which is similar to the standard deviation of the surface currents (Figure 3a), reflecting the coastal boundary effects on the sub-inertial surface currents (Figure 3b). The weak variance at the eastern boundary of the study domain is caused by the reduced radio signals.

The magnitudes of the clockwise diurnal surface currents are enhanced near the coast and decreased away from the coast (Figure 3c), which is closely related to diurnal development of the marine boundary layer associated with diurnal land-sea breezes.

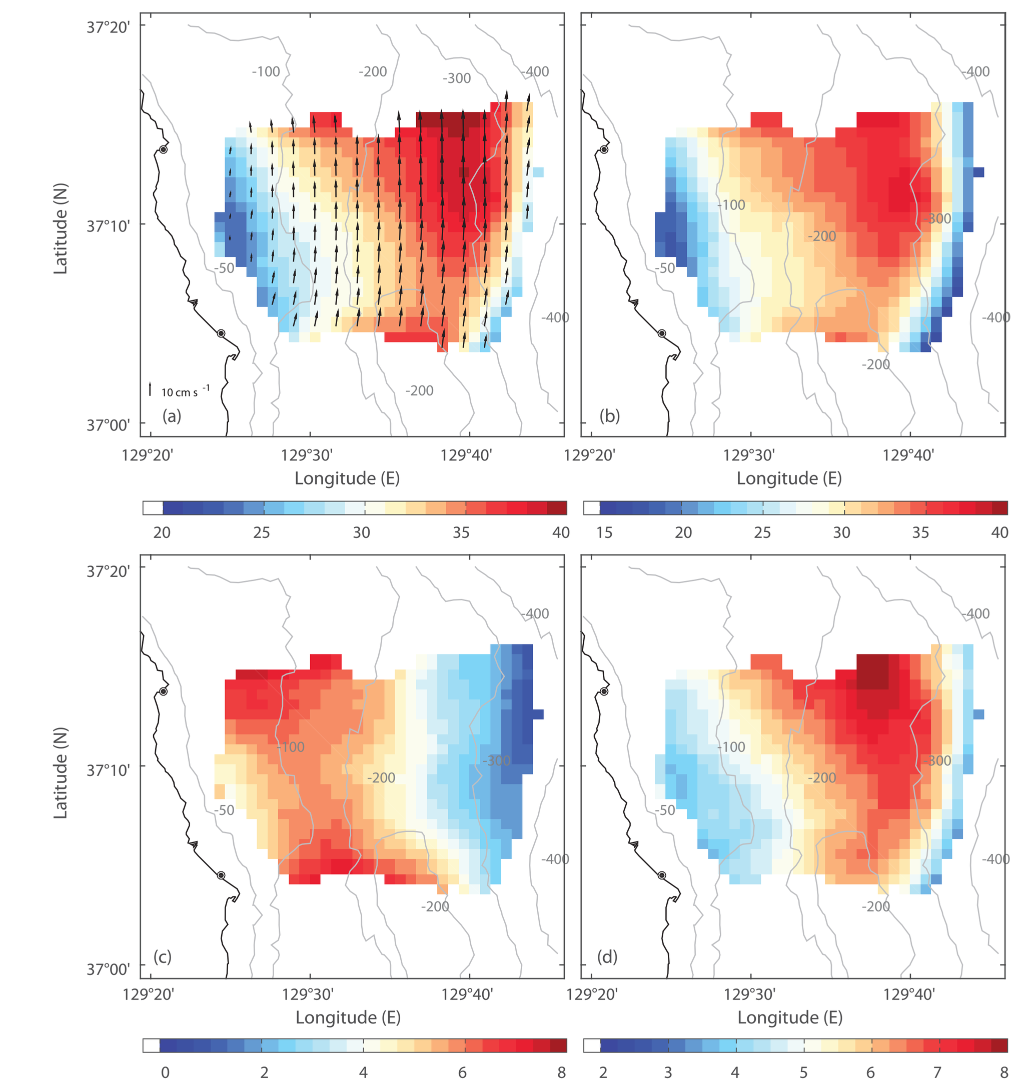

Figure 3: (a) Temporal mean ($\sigma = 0$ cpd) and standard deviation of surface currents ($\mathrm{cm\,s^{-1}}$) are marked with the black arrows and color-coded patches, respectively. The temporal mean of surface currents is plotted at every 2 km to minimize overlapping of the arrows. (b) to (d): Magnitudes [$\mathrm{cm\,s^{-1}}$] of the hourly surface currents for a period of one year (2013) (b) in the non-zero low-frequency band ($0 < |\sigma| \leq 0.2$ cpd) on both rotations, (c) at the clockwise diurnal frequency ($\sigma = -1$ cpd), and (d) in the clockwise near-inertial frequency band ($-1.4 \leq \sigma \leq -1.2$ cpd). The bottom bathymetry is contoured at 50 m, 100 m, 200 m, 300 m, and 400 m.

The near-inertial surface currents in the study domain are characterized with dominant clockwise super-inertial variance (Figure 1a), which is consistent with the observed near-inertial currents from the in-situ buoy located at approximately 50 km northwest of the study area (D in Figure 2b). These super-inertial currents have been interpreted as the onshore propagating (internal) near-inertial waves which are generated offshore.

The magnitudes of the clockwise near-inertial surface currents are reduced near the coast and enhanced offshore, which is associated with the influence of coastal boundaries (e.g., bottom bathymetry and coastline) on the near-inertial motions called 'coastal inhibition' (Figure 3d).

We examine the near-inertial variance modulated by background vorticity with the amplitudes of the surface currents at two locations of A and B (Figure 2b) at trial frequencies within the clockwise near-inertial frequency band ($|\sigma - f_c| \leq 0.5$ cpd), which are estimated using a least-squares fit (Figures 4c and 4d). Rossby number (R_o) and stream function (ψ) represent the rotation of the current field as a complementary tool. Note that $\psi < 0$ and $R_o < 0$ indicate clockwise rotational flows (red), and $\psi > 0$ and $R_o > 0$ indicate counter-clockwise rotational flows (blue). Since the Rossby number and stream function are derivative and integrated quantities, respectively, the spatial structure of the stream function can be smoother than that of the Rossby number. The scaled stream function (ψ/ψ^*, where $\psi^* = 500\ \mathrm{m^2\,s^{-1}}$) and the scaled Rossby number (R_o/R_o^*, where $R_o^* = 2$) at two locations of A and B (Figure 2b) are coherent with the enhanced amplitudes at the trial frequencies. Note that the stream function and Rossby number are scaled with constant values to present them in the same panel.

Variance in the wavenumber domain

Overall, the wavenumber-domain energy spectra of surface currents have decay slopes between k^{-2} and k^{-3} (Figures 6a and 6c) with slight differences in the averaging direction, consistent with the energy spectra of coastal surface currents reported elsewhere. The seasonally averaged wavenumber-domain spectra have slightly steeper decay slopes in winter than in summer and higher variance in summer than in winter (Figures 6b and 6d), which an opposite pattern of the submesoscale processes associated with the seasonal mixed layer. The non-seasonal and persistent regional mesoscale currents and their branches near the coast may affect the generation of submesoscale frontogenesis.

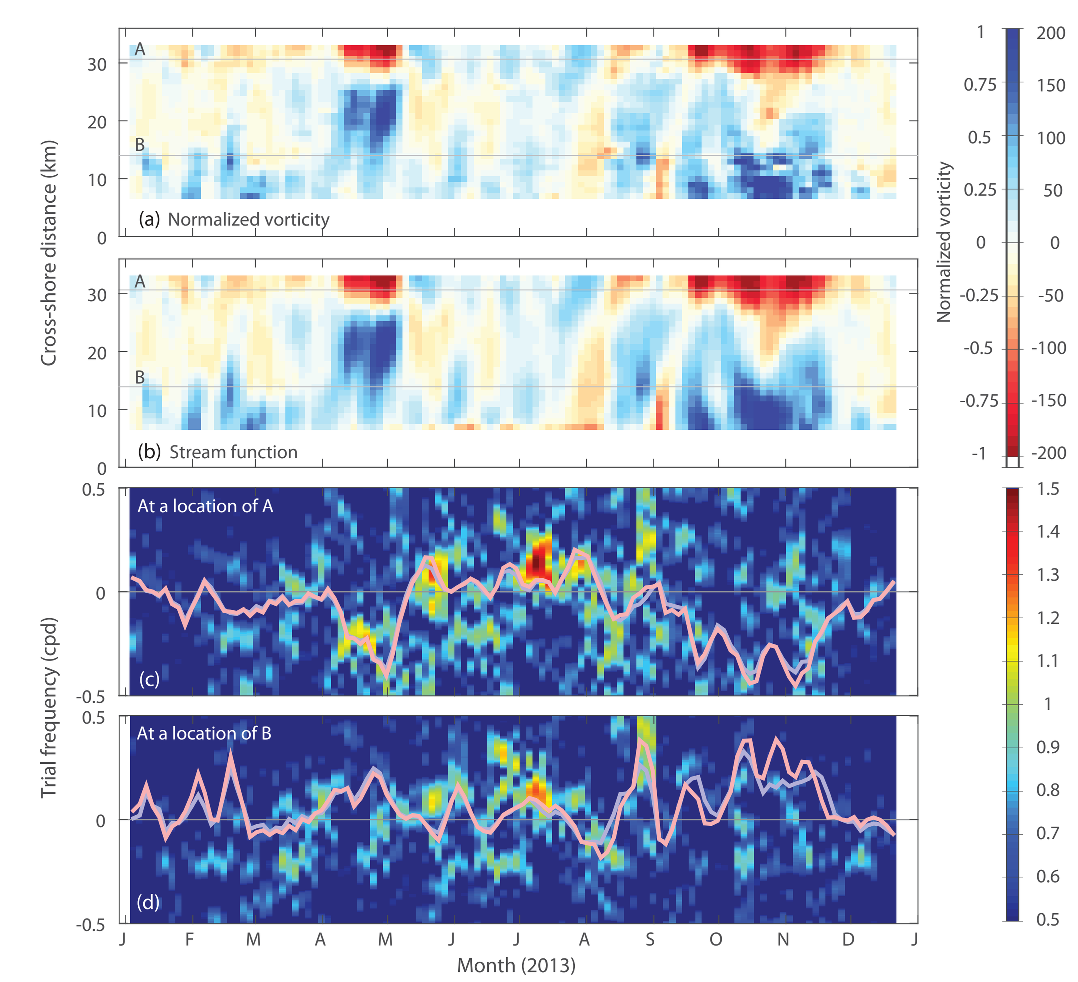

Figure 4: Cross-shore time series of (a) the Rossby number ($R_o = \zeta/f_c$), i.e., normalized vorticity and (b) the stream function (ψ; $\mathrm{m^2\,s^{-1}}$) along the cross-shore line in Figure 2b. (c) and (d): Time series of variance ($\mathrm{cm^2\,s^{-2}}$; $\log_{10}$ scale) of the surface currents at the trial frequency within the clockwise near-inertial frequency band ($|\sigma - f_c| \leq 0.5$ cpd), obtained at two sampling locations of A and B in Figures 4a and 4b, respectively. The pink and light purple curves indicate the scaled stream function (ψ/ψ^*, where $\psi^* = 500\ \mathrm{m^2\,s^{-1}}$) and the scaled Rossby number (R_o/R_o^*, where $R_o^* = 2$) at each location, respectively. Note that $\psi < 0$ and $R_o < 0$ denote clockwise rotational flows (red) and $\psi > 0$ and $R_o > 0$ denote counter-clockwise rotational flows (blue). The individual estimates are based on a 9-day moving time window along with a 3-day time increment.

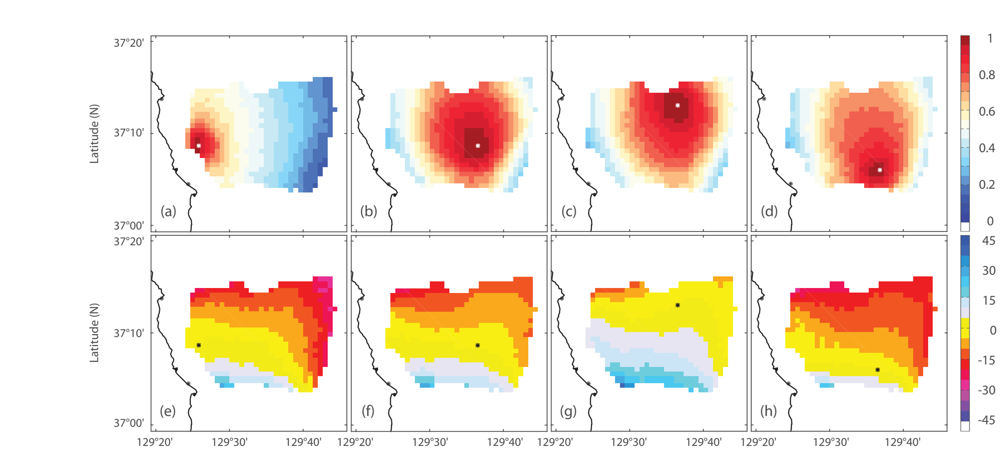

Figure 5: Spatial coherence of the clockwise near-inertial surface currents ($|\sigma - f_c| \leq 0.3$ cpd) between a reference location (a white star for magnitudes and a black star for phases) and the rest of grid points. (a) to (d): Magnitudes. (e) to (h): Phases (degrees).

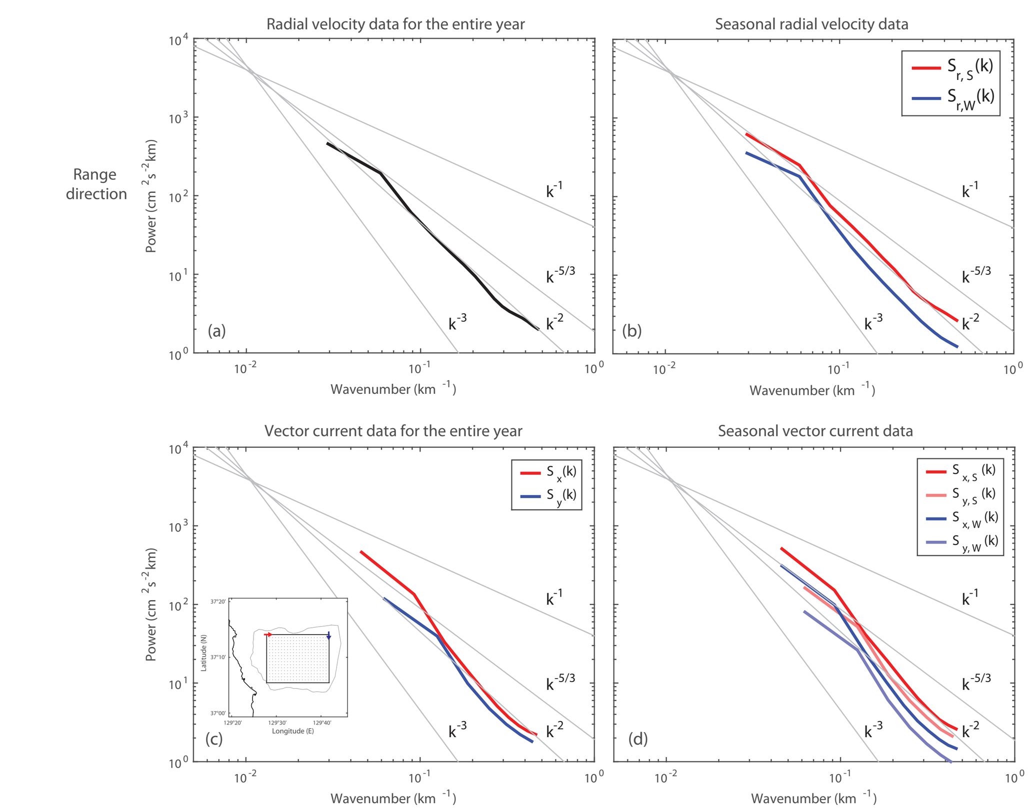

Figure 6: (a) and (b): Wavenumber-domain energy spectra of hourly radial velocities in the range direction [$S_{r,S}(k)$ for summer (red) and $S_{r,W}(k)$ for winter (blue)]. (c) and (d): Wavenumber-domain energy spectra of the hourly vector currents in the along-shore (y) and cross-shore (x) directions, respectively, for a period of one year (2013) and individual seasons (summer and winter). Gray auxiliary lines indicate the decay slopes of k^{-1}, $k^{-5/3}$, k^{-2}, and k^{-3}.

Concluding remarks

We examined the spectral contents of the hourly coastal surface currents on a 1-km spatial resolution in the frequency and wavenumber domains. The surface currents observed for a period of one year exhibit the dominant variance in the low-frequency (longer than 2 days), diurnal, and near-inertial frequency bands. The low-frequency surface currents have more consistent variability with regional geostrophic currents in summer than those in winter since relatively weaker wind conditions and shallower mixed layer are expected during summer. The diurnal surface circulation contain components coherent with diurnal land-sea breezes related to the development of the diurnal marine boundary layer. Additionally, super-inertially shifted clockwise surface currents exhibit the on-shore phase propagations along with decreasing amplitudes as a part of coastal inhibition due to coastal boundary effects on the near-inertial currents. The wavenumber-domain energy spectra of surface currents have decay slopes between k^{-2} and k^{-3}. Their seasonal decay slopes are slightly steeper in winter than in summer, which can be interpreted as the influence of both surface frontogenesis due to regional mesoscale eddies with weak seasonality and baroclinic instability associated with the seasonal mixed layer and vertical fluctuations modulated by its harmonic frequencies.

Acknowledgement

Jang Gon Yoo and Sung Yong Kim are supported by a research project titled by 'Research for Applications of Geostationary Ocean Color Imager' through Korea Institute of Marine Science and Technology Promotion (KIMST), Ministry of Oceans and Fisheries and a grant through the Disaster and Safety Management Institute, Ministry of Public Safety and Security (MPSS-CG-2016-05), Republic of Korea

References

[1] S. Y. Kim, E. J. Terrill, and B. D. Cornuelle. Mapping surface currents from HF radar radial velocity measurements using optimal interpolation. *J. Geophys. Res.*, 113, 2008.

[2] Byoung-Ju Choi, Do-Seong Byun, and Kang-Ho Lee. Satellite-altimeter-derived East Sea surface currents: Estimation, description and variability pattern. *The Sea, J. Korean Soc. Oceanogr.*, 17(4):225–242, 2012.